Title

Short peptides self-assemble to produce catalytic amyloids.

Journal

Nature Chemistry, 6(4)

Authors

Rufo, Caroline
Moroz, Yurii
Moroz, Olesia
et al.

Publication Date

2014-04-01

DOI

10.1038/nchem.1894

Peer reviewed

HHS Public Access

Author manuscript

Nat Chem. Author manuscript; available in PMC 2014 October 01.

Published in final edited form as:

Nat Chem. 2014 April ; 6(4): 303–309. doi:10.1038/nchem.1894.

Short peptides self-assemble to produce catalytic amyloids

Caroline M. Rufo[1,†], **Yurii S. Moroz**[1,†], **Olesia V. Moroz**[1,†], **Jan Stöhr**[2], **Tyler A. Smith**[1], **Xiaozhen Hu**[3], **William F. DeGrado**[3,*], and **Ivan V. Korendovych**[1,*]

[1]Department of Chemistry, Syracuse University, Syracuse, NY 13244, USA

[2]Institute for Neurodegenerative Diseases and Department of Neurology, University of California – San Francisco, San Francisco, CA 94143, USA

[3]Department of Pharmaceutical Chemistry, University of California – San Francisco, San Francisco, CA 94158, USA

Abstract

Enzymes fold into unique three-dimensional structures, which underlie their remarkable catalytic properties. The requirement to adopt a stable, folded conformation is likely to contribute to their relatively large size (> 10,000 Dalton). However, much shorter peptides can achieve well-defined conformations through the formation of amyloid fibrils. To test whether short amyloid-forming peptides might in fact be capable of enzyme-like catalysis, we designed a series of 7-residue peptides that act as Zn^{2+}-dependent esterases. Zn^{2+} helps stabilize the fibril formation, while also acting as a cofactor to catalyze acyl ester hydrolysis. These results indicate that prion-like fibrils are able to not only catalyze their own formation – they also can catalyze chemical reactions. Thus, they might have served as intermediates in the evolution of modern-day enzymes. These results also have implications for the design of self-assembling nanostructured catalysts including ones containing a variety of biological and nonbiological metal ions.

The mechanisms by which proteins evolved to possess enzymatic activity remain a major unanswered question. An enzyme's amino acid sequence underlies its ability to fold into a native structure, which positions and tunes the dynamics of functional groups required for binding and catalysis. Modern day enzymes are generally at least 100 residues in length, which is close to the chain length required to create a well-defined hydrophobic core in a globular protein. A protein of this length, however, would have an astronomically large number of possible sequences, and it is unclear how nature might have tested sufficient numbers of permutations to find one capable of folding and function.

Correspondence and requests for materials should be addressed to I.V.K. (ikorendo@syr.edu) or W.F.D. (william.degrado@ucsf.edu).

†These authors contributed equally to this work.

Author contributions: C.M.R., Y.S.M., O.V.M., J.S., T.A.S. and X.H. performed the experiments and analyzed the data, W.F.D. and I.V.K. conceived and designed the experiments and wrote the paper. All authors discussed the results and commented on the manuscript. C.M.R., Y.S.M. and O.V.M.

Supplementary information and chemical compound information are available in the online version of the paper.

Competing financial interests: The authors declare no competing financial interests.

This apparent paradox has led to the suggestion that the earliest proteins might have been formed from short peptides or polymers with repeating amino acid sequences that relied on self-assembly to achieve a folded structure[1, 2]. Indeed, simple heptapeptides with alternating apolar and polar residues self-assemble into extended beta sheets stabilized through intermolecular association of the apolar residues in the sequence repeat[3]. Moreover, structural characterization of short amyloid-forming peptides has revealed a myriad of conformational variations on the basic cross-β conformation[4–6]. Thus, it is possible that the first primitive protein enzymes were short peptides with amyloid structures providing the frameworks to support their catalytic activities.

Metals also might have figured largely in the emergence of catalytic activity of proteins[7, 8]. Not only do transition metal ions help catalyze reactions, but they also can influence the folding of proteins through the interaction with ligating sidechains. We therefore explored the design, metal interactions, and catalytic properties of Zn^{2+}-binding amyloidogenic peptides. Zn^{2+} was chosen as a cofactor given its high abundance and frequent occurrence in modern metal-dependent hydrolases such as carbonic anhydrase and metalloproteases. The Zn^{2+} ion lowers the pK_a of a bound water, stabilizing and positioning hydroxide for nucleophilic attack of the substrate. The Zn^{2+} binding site in enzymes often contains two His ligands projecting from positions *i* and *i+2* of a β-sheet; a third His ligand from a neighboring strand completes the primary ligand environment. This very simple inter-strand 3-His metal-binding site is observed in proteins such as erythrocyte carbonic anhydrase (Fig. 1a)[9]; similarly two His residues from neighboring positions of β-strands are seen in the amyloid-like β-solenoid structure of an archaeal γ-carbonic anhydrase[10]. Additionally, general acid/bases from neighboring sidechains serve as secondary ligands and assist protonation/deprotonation events in catalysis. We therefore asked whether a similar site might be created within the β-sheet-forming minimalist heptapeptide sequence (LKLKLKL). This and related peptides have alternating hydrophobic residues, which creates an amphiphilic β-strand that further associates via hydrophobic interactions to form extended amyloid β-structures[11, 12]. Considerable sequence variation is tolerated so long as the hydrophobic periodicity is retained[13, 14]. We retained the apolar Leu residues to drive assembly while the Lys sidechains at positions 2, 4, and 6 were changed to polar residues capable of supporting transition metal ion binding and catalysis. Zn^{2+}-binding His residues were placed at positions 2 and 4; at position 6 (Fig. 1b) we explored acidic (Asp, Glu), neutral (Gln, Tyr), and basic residues with various pK_a values (His, Lys, Arg).

Results and discussion

Hydrolytic enzymes perform a diverse set of functions ranging from amide, ester, or lipid hydrolysis to catalyzing the equilibration between CO_2 and bicarbonate. Despite such diversity many hydrolytic enzymes are assayed and benchmarked using a simple chromogenic substrate - *p*-nitrophenylacetate (*p*NPA). Therefore, we chose this substrate to allow for comparison with natural enzymes and various designed protein catalysts. Most of the seven original designs displayed measurable activity over the buffer control (pH 8 in the presence of 1 mM $ZnCl_2$) in the initial screening for *p*NPA hydrolysis as shown in Table 1. The dependence of the initial rate of the reaction on substrate concentration for a typical peptide (**7**, LHLHLRL) is consistent with the Michaelis-Menten model, with $k_{cat} = 3.2 \pm 0.4$

$\times 10^{-2}$ s^{-1}, K_M = 1.8 ± 0.4 mM, and a catalytic efficiency k_{cat}/K_M = 18 ± 4 M^{-1} s^{-1} (Fig. 2a, Table 1).

The activity of **7** is strictly zinc-dependent, and no significant activity above the background is observed in the absence of Zn^{2+}. The catalytic activity also showed a marked dependence on the nature of the residue at position 6. Interestingly, peptide **3**, with an amyloidogenic glutamine residue at this position was the most active with k_{cat}/K_M = 30 ± 3 M^{-1} s^{-1}. Peptides with Asp, Glu or His residues at position 6 (**1, 2, 5**, respectively) had little to no activity, possibly because these sidechains compete with the His residues at positions 2 and 4 for binding to the metal ion at catalytically inactive sites.

Structure-activity relationships

Intrigued by the finding that a potentially amyloid-promoting Gln residue enhanced catalytic activity we varied the hydrophobic Leu residues that were expected to stabilize the β-sheet association. Replacement of the Leu residues with residues of greater β-sheet propensity[15, 16], Ile or Val, produced peptides **9** (IHIHIRI) and **10** (VHVHVRV) with almost 50% increase in activity as compared to **7**. Conversely, replacement of Leu with Ala, a residue with both lower hydrophobicity and weaker β-sheet-forming propensity, gave a peptide (**8**) almost inactive as an esterase. The terminal acetyl and carboxamide groups also appeared to be important for activity, as the peptide lacking these groups (**14**) was catalytically inactive. These observations are in good agreement with previous studies that showed that subtle modifications of secondary structure in short peptide catalysts lead to substantial improvements in activity and substrate specificity[17, 18].

The activity of **9** (IHIHIRI) could be further increased by inclusion of Gln at position 6, which had already been shown to increase activity in the leucine-containing peptides. The effects of introducing β-branched amino acids and glutamine are additive: the peptide containing both isoleucines in its hydrophobic core and Gln in position 6 (**11**, IHIHIQI) is 3.5-fold more active than **7** (Table 1) and reaches a k_{cat}/K_M value of 360 ± 30 M^{-1} s^{-1} at pH 10.3 (Fig. 2b). The catalysis follows Michaelis-Menten kinetics, and no product inhibition was observed over 20 turnovers. A similar effect, albeit to a lower extent, was observed when Gln was introduced into the valine-containing peptide **10**. Interestingly, in both cases the gain in catalytic efficiency comes from the decrease in K_M rather than improvement in k_{cat}. The activity of **11** is more than 100-fold greater in the presence than the absence of Zn^{2+}, showing that the activity does not arise from simple imidazole catalysis (which is considerably lower[19, 20] than the rate measured for Zn^{2+}-**11** fibrils). Also, the activity of fibrils formed by **11** is more than 10-fold greater than those of non-metal based esterases identified in combinatorial libraries by Hecht et al.[21, 22] and designed by Baltzer et al.[23] and Mayo et al.[20] Fibrils formed by **11** are over an order of magnitude more active than de novo designed, zinc-binding trimeric coiled coils reported by Pecoraro et al.[24] and are on par with the most active to date zinc-protein complex reported by Kuhlman and coworkers[25]. Moreover, the activity of **11** on a weight basis is greater than that of carbonic anhydrase, which catalyzes *p*NPA hydrolysis with k_{cat}/K_M = 2550 M^{-1} s^{-1}.[26] Such remarkable efficiency is due to the small size of the active unit in **11** (likely a dimer of 7-residue peptides), while the protein is at least 15-fold larger in molecular weight.

The proper coordination of the metal ion is also crucial, as a single mutation of either histidine residue to alanine results in at least 60-fold decrease in esterase activity (Table 1). Further examination of the catalytic activity of **11** (IHIHIQI) as a function of Zn^{2+} concentration showed that the activity increased linearly until a stoichiometry of approximately 1:2 (zinc to peptide) was reached, after which no significant increase was observed (Fig. 2c). This finding is consistent with the design in which two peptides cooperate to form the active catalyst. The pH activity profile of **11** is consistent with two protonation/deprotonation steps with pK_a's of 7.1 ± 0.4 and 9.3 ± 0.1 (Fig. 2b). It is possible that one pK_a reflects deprotonation of a His sidechain to free it for ligation to Zn^{2+}, while the higher pK_a reflects the pK_a of Zn^{2+} water/hydroxide, although further work will be required to confirm this suggestion. Similar two-step protonation behavior was observed for other active peptides (Supplementary Fig. S1). Catalytic efficiency of the fibrils does not depend on the initial concentration of the monomeric peptide used for assembly; the reaction is first order in peptide in the concentration range studied (24-200 μM) (Fig. 2d).

Characterization of the active species

Having established that the peptides are catalytically active, we used circular dichroism (CD) spectroscopy and IR to show that they adopted a β-sheet conformation in the presence of Zn^{2+}. Also, thioflavin T (ThT) binding and negative stain transmission electron microscopy (TEM) was used to probe fibril formation. The Leu-containing peptide **7** adopts a β-sheet structure in a strictly Zn^{2+}-dependent manner. In the absence of Zn^{2+} the peptide displays a CD spectrum characteristic of random coils, but upon addition of the metal ion a spectrum typical of the cross-β configuration is observed (Fig. 3a). Comparison of spectra at pH 2 and 8 showed that Zn^{2+}-triggering of β-sheet structure occurred only at pH 8, where the His ligands should be deprotonated and available to complex metal ions. Similar results were seen for the remaining (**1–6**) peptides examined (Supplementary Fig. S2). Interestingly, the nearly inactive peptide **5** (LHLHLHL) showed a β-sheet-like CD spectrum even in the absence of Zn^{2+}. This finding suggests that this peptide might be pre-organized into a structure that does not support catalysis or, as mentioned above, the additional His competes for catalytically competent Zn^{2+} binding. Interestingly, the most catalytically active Leu-to-Ile substituted peptides (**9, 11**) showed a β-sheet-like CD spectrum at pH 8, even in the absence of Zn^{2+} (Fig. 3b), suggesting that this substitution promoted the formation of a catalytically competent structure. The position of the amide I' IR band of the catalytically active peptides (**7, 9, 11**) near 1626 cm^{-1} further supported these conclusions[27] (Supplementary Fig. S3). The CD spectra of **9** and **11** at pH 8 in the presence of Zn^{2+} show highly intense minima around 207 nm. Similar spectra were found with fibrils formed by peptides derived from a mouse prion protein and might be indicative of β-structures in readily formed amyloid complexes.[28, 29]

Physical separation methods showed that the active catalyst is assembled into very high molecular weight aggregates. Extensive dialysis of **11** using a 10K MWCO membrane against zinc-containing buffer showed that the catalytically active species was unable to diffuse through the membrane. Furthermore, when the aggregated peptides were filtered through membranes with 0.1, 0.22 or 0.45 μm pores the filtrate was at least 800-fold less active that the starting suspension (Fig. 4a). Moreover, ThT binding and TEM identified

these catalytically active aggregates as fibrils. ThT binds to fibrils in preference to prefibrillar oligomeric states or monomeric peptides, and the binding is conveniently evaluated through a large enhancement in the fluorescence of this dye. Indeed, ThT fluorescence increased significantly in the presence of Zn^{2+} at pH 8, and the most active peptides tended to have the greatest fluorescence enhancement in this assay (Fig. 4b). This finding was confirmed by TEM images of **7, 9** and **11** that reveal extended amyloid-like fibrils (Fig. 4c-f, Supplementary Figs. S4, S5).

Formation of amyloid-like structures often requires appropriate nucleation and thus a lag phase is frequently observed. We have characterized the activity of designed peptides at various time points after addition of Zn^{2+} and the concomitant pH increase. Peptides **4, 6** and **7**, which have a Leu core, show a lag phase, reaching their maximum activity at around 24 hours. Introducing Gln into the sequence and, especially, substituting leucines with isoleucines drastically diminishes the fibrillation time and the maximum activity is achieved with no need for longer incubation (Supplementary Fig. S6). This observation is consistent with the results of centrifugation studies conducted to determine the fraction of large aggregates. The solutions of representative peptides at pH 8 in the presence of Zn^{2+} were subjected to centrifugation at 100,000 g for 1 hour immediately after preparation and following 24-48 hours of incubation at room temperature. Immediately on addition of the pH 8 buffer containing Zn^{2+} **11** oligomerizes essentially completely (at least 95%) whereas approximately 55% of peptide **7** is still present in the form of low molecular weight species as judged by their UV absorbance. After a 24 hour incubation the soluble fraction of **7** drops to approximately 20% and remains constant thereafter (Supplementary Fig. S7). TEM studies provide additional insight into oligomerization of **7**: freshly produced samples show protofibrils that fully mature after prolonged incubation (Fig. 4c-d). Importantly, non-fibril forming peptide **8** showed no decrease in soluble fraction absorbance indicating that no oligomeric species were formed.

Finally, no strong evidence for β-sheet structure based on CD spectra was observed for the catalytically inactive peptide **14**, which has unblocked N- and C-termini. Moreover, under conditions where active peptides showed extensive fibril formation, **14** did not produce fibrils as judged by TEM. This finding might indicate that the β-strands in the active fibrils are arranged in parallel fashion – in such a scenario neutralizing the terminal groups by acetylation and amidation would stabilize the structure by eliminating unfavorable electrostatic interactions between charged end groups. However, structural studies will be required to confirm this topology and detailed structure of the fibrils.

Metal coordination sphere

To probe the coordination sphere of the metal ion in the active catalyst we studied fibrillation of **9** and **11** in the presence of cobalt ions. Co^{2+} triggers fibril formation in a manner analogous to zinc while providing easy spectroscopic insight into the metal coordination geometry. The breadth and intensity of the d-d transition band in the UV-vis spectrum of the fibrils formed by **9** and **11** in the presence of cobalt excludes the possibility of octahedral ligand arrangement and are consistent with tetrahedral cobalt coordination[30] (Supplementary Fig. S8). TEM studies show that the morphology of the fibrils formed in the

presence of cobalt is not altered compared to the zinc bound fibrils (Supplementary Fig. S9). These findings are in good agreement with the results of computational modeling of the assembly using Rosetta software (see Supplementary Information for details). The energy-minimized model of the fibrils formed by **11** in the presence of Zn^{2+} ions is presented in Fig. 1c-e. It shows a well-packed hydrophobic core formed by isoleucine residues; the histidine residues support a tetrahedral zinc coordination sphere.

Synergistic interactions between peptides

The above studies show that relatively simple design principles are needed to discover amyloid-like peptides that display very substantial catalytic activity for ester hydrolysis. More than half of the 14 peptides studied here were active, and the activity could be easily enhanced by following simple physical principles such as enhancing the amyloidogenic potential and β-sheet-forming properties of the peptides. This is but a small fraction of the $20^7 = 1.28 \times 10^9$ possible peptide sequences that could be composed of the 20 naturally occurring amino acids, or $3^7 = 2{,}187$ if one were to restrict the alphabet to just three amino acids, such as His, Ile, and Gln in the most active peptides studied here. It remains to be seen how many other activities could be discovered from relatively simple libraries in the absence and presence of other biological and non-biological metal ions. Furthermore, diversity could be greatly enhanced (by a factor of $(n+n^2)/2$, where n is the number of peptides in the library) if the peptides were considered in binary mixtures of only two peptides. To test the possibility that a mixture of two peptides might have synergistic interactions we mixed the two peptides that showed moderate activity in the initial screening – **4** and **7**. To assure mixing of the individual peptides within the fibril, they were mixed in different proportions in aqueous HCl (10 mM) and then diluted into Zn^{2+}-containing (1 mM) TRIS buffer at pH 8 to ensure effective mixing of peptides prior to formation of fibrils. The activity profile shows synergy between **4** and **7** (Fig. 5a) with maximum esterase activity observed when the peptides were mixed relative to the individuals alone. The experimental data are well described by a simple model, where a dimer is the active species and the peptides are randomly distributed in the fibril. By contrast, if fibrils of the individual peptides were allowed to form first, and then they were mixed, no synergy was observed. Instead a linear decrease in activity was seen upon increasing the ratio of **4** relative to **7** (Fig. 5b). Detailed structural studies will be necessary to elucidate the composition and geometry of the active unit as the data could be also fit to a more complex oligomerization (e.g. peptide trimer constituting the active species) models.

Conclusion

Here, we showed that small 7-residue amyloid-forming peptides designed from the first principles form efficient catalysts of ester hydrolysis. This observation supports a potential link between amyloid assemblies and the emergence of protein catalysts during the evolution of enzymes. The ability to screen multiple stable arrangements of functional groups in a single fibril provides essentially limitless opportunities for high-throughput screening for functional activity by simply mixing peptides with different sequences. We expect this approach to be a tool for designing new materials capable of performing catalysis on both natural and non-natural substrates. This work also might have implications to the

mechanisms of amyloid toxicity; zinc and copper ions alter the kinetics and nature of the cellular prion protein (PrR^C)[31, 32]. Moreover, it has been suggested that amyloid-forming Aβ-peptides might form complexes with Cu^{2+} that mediate formation of reactive oxygen species (ROS) in an incompletely understood manner[33–35]. The ease with which we were able to discover robust and reproducible metalloprotein catalysts would suggests that one should further consider toxic catalytic activities as one possible source of amyloid toxicity.

Methods

Peptide synthesis

The peptides were synthesized by manual fluorenylmethyloxycarbonyl (Fmoc) solid phase synthesis at elevated temperature using our previously reported protocol optimized for hydrophobic peptides[36]. Cleavage of the peptides from resin and side chain deprotection was simultaneously achieved by treatment with a mixture of trifluoroacetic acid (TFA)/H_2O/ triisopropyl silane (TIS) (95:2.5:2.5, v/v) for 2 hours at room temperature. The crude peptides were precipitated and washed with cold methyl-*tert*-butyl ether, and purified on a preparative reverse phase HPLC system (Varian ProStar 210) with a C4 preparative column (Vydac), using a linear gradient of solvent A (0.1% TFA in Millipore H_2O) and solvent B (90% CH_3CN, 10% H_2O, 0.1% TFA). The identities and the purities of the purified peptides were confirmed by MALDI-TOF mass spectrometry using a Bruker Autoflex III Smartbeam MALDI-TOF mass spectrometer. Purity of the obtained peptides was additionally evaluated on a Shimadzu Prominence UFLC instrument with an analytical Zorbax Eclipse XDB-C18 column (4.6 mm×150 mm).

Preparation of peptide stocks and solutions

Purified lyophilized peptides were dissolved in 10 mM hydrochloric acid to make a 1.1 mM stock solution. Concentration was determined using an Agilent 8453 UV-Vis spectrophotometer using absorbance at 214 nm. Extinction coefficients for the peptides at this wavelength were calculated using literature values[37]. The pH 8 working stock solution of peptides was prepared by mixing 180 μL of the pH 2 stock with 20 μL of isopropanol followed by addition of 1.8 mL of buffer (25 mM TRIS pH 8 containing 1 mM $ZnCl_2$). Adherence to this protocol assured reproducibility between runs and provided a standard method to compare different peptides. The pH 2 stock solution was stable for at least a week, the working stock solution of peptides at pH 8 was prepared immediately before experiments.

Kinetic assays

Kinetic measurements were done on a Thermo Labsystems Multiskan Spectrum plate reader monitoring absorbance of the product (*p*-nitrophenol) at 348 nm and 405 nm at 22 °C in 96-well plates. *p*-Nitrophenylacetate was used from a 0.1 M stock in acetonitrile (the final acetonitrile content was 2 % in all reaction mixtures). 150 μL of freshly prepared substrate solution in 25 mM TRIS (pH 8), 1 mM $ZnCl_2$ (to the final substrate concentration of 0.195 - 0.75 mM) was added to 50 μL of buffered (25 mM buffer) peptide stock solution at pH 8 (to final peptide concentration of 24 μM). Extinction coefficients of 1,700; 4,300; 9,100; 12,700; and 16,600 M^{-1} cm^{-1} were used to determine the product concentration at pH of 6,

6.5, 7, 7.5, and 8, respectively, at 405 nm. An extinction coefficient of 18,700 M^{-1} cm^{-1} was used at pH 8.5 and above at 405 nm. The extinction coefficients reported above were experimentally obtained by measuring UV-vis spectra of *p*-nitrophenol in buffers at different pH values. The *p*-nitrophenol solutions were obtained by 40-fold dilution of 2.5 mM stock solution of *p*-nitrophenol in acetonitrile into the appropriate buffers. The reported results were obtained by averaging of at least three independent measurements. Kinetic parameters (k_{cat} and K_M) were obtained by fitting the data to the Michaelis-Menten equation $\{v_0=k_{cat}[E]_0[S]_0/(K_M+[S_0])\}$. k_{cat}/K_M values were obtained by fitting the linear portion of the Michaelis-Menten plot to $v_0=(k_{cat}/K_M)[E]_0[S]_0$. pH profile studies were done on an Agilent 8453 spectrophotometer monitoring absorbance of the product at 405 nm at 22°C using a 1 cm quartz cuvette. 150 μL of buffer solution (the following buffers were used at the concentration of 25 mM: MES (pH 6-6.5), HEPES (pH 7-7.5), TRIS (pH 8-8.5), TAPS (pH 9-9.5) and CAPS (pH 10-10.5) was added to 50 μL of peptide solution (in 25 mM TRIS pH 8 containing 1 mM $ZnCl_2$) in a cuvette, followed by addition of 2 μL of 20 mM pNPA in acetonitrile. Due to precipitation of zinc hydroxide at high pH, the added buffers at pH values of 8 and below contained 1 mM $ZnCl_2$, the buffers at pH values of 8.5-9 contained 0.5 mM $ZnCl_2$ (the final Zn^{2+} was 0.625 mM) and at the pH values of above 9.5 the added buffer contained no zinc salts (the final Zn^{2+} was 0.25 mM). The pH changes due to mixing of different buffer volumes at different pH values were accounted for. The product formation was monitored for 5 min every 30 sec. The pH profile data were fit to the following equation:

$$\frac{k_{cat}}{K_M}=\frac{\left(\frac{k_{cat}}{K_M}\right)_{max1}10^{-pK_{\alpha1}}}{10^{-pH}+10^{-pK_{\alpha1}}}+\frac{\left(\frac{k_{cat}}{K_M}\right)_{max2}10^{-pK_{\alpha2}}}{10^{-pH}+10^{-pK_{\alpha2}}}$$

where k_{cat}/K_M is the observed enzymatic efficiency at a particular pH value, the pK_{a1} and pK_{a2} are the respective pK_a's for the two protonation/deprotonation steps and $(k_{cat}/K_M)_{max1}$ and $(k_{cat}/K_M)_{max2}$ are the corresponding maximum activities.

Supplementary Material

Refer to Web version on PubMed Central for supplementary material.

Acknowledgments

We thank Korrie L. Mack, Genevieve G. Ariotti, Robert P. Doyle, Mathew M. Maye and Robert P. Smith for technical assistance and discussions. This work was in part supported by grant number GM54616 from the NIH to W.F.D., grant number 1332349 from NSF-EFRI and ORAU Ralph E. Powe Junior Faculty Enhancement award to I.V.K. We also acknowledge support from the MRSEC program of the NSF, grant DMR-1120901.

References

1. Greenwald J, Riek R. On the possible amyloid origin of protein folds. J. Mol. Biol. 2012; 421:417–426. [PubMed: 22542525]
2. Carny O, Gazit E. A model for the role of short self-assembled peptides in the very early stages of the origin of life. FASEB J. 2005; 19:1051–1055. [PubMed: 15985527]
3. DeGrado WF, Lear JD. Induction of peptide conformation at apolar/water interfaces: A study with model peptides of defined hydrophobic periodicity. J. Am. Chem. Soc. 1985; 107:7684.

4. Eisenberg D, Jucker M. The amyloid state of proteins in human diseases. Cell. 2012; 148:1188–1203. [PubMed: 22424229]
5. Colletier JP, et al. Molecular basis for amyloid-beta polymorphism. Proc. Natl. Acad. Sci. U.S.A. 2011; 108:16938–16943. [PubMed: 21949245]
6. Nowick JS. Exploring β-sheet structure and interactions with chemical model systems. Acc. Chem. Res. 2008; 41:1319–1330. [PubMed: 18798654]
7. Wachtershauser G. Before enzymes and templates: theory of surface metabolism. Microbiol. Rev. 1988; 52:452–484. [PubMed: 3070320]
8. Rode BM, Son HL, Suwannachot Y, Bujdak J. The combination of salt induced peptide formation reaction and clay catalysis: a way to higher peptides under primitive earth conditions. Orig. Life Evol. Biosph. 1999; 29:273–286. [PubMed: 10465717]
9. Christianson DW, Fierke CA. Carbonic anhydrase: Evolution of a zinc binding site by nature and by design. Acc. Chem. Res. 1996; 29:331–339.
10. Iverson TM, Alber BE, Kisker C, Ferry JG, Rees DC. A closer look at the active site of gamma-class carbonic anhydrases: high-resolution crystallographic studies of the carbonic anhydrase from Methanosarcina thermophila. Biochemistry. 2000; 39:9222–9231. [PubMed: 10924115]
11. West MW, et al. De novo amyloid proteins from designed combinatorial libraries. Proc. Natl. Acad. Sci. U.S.A. 1999; 96:11211–11216. [PubMed: 10500156]
12. DeGrado WF, Wasserman ZR, Lear JD. Protein design, a minimalist approach. Science. 1989; 243:622–628. [PubMed: 2464850]
13. Schneider JP, et al. Responsive Hydrogels from the Intramolecular Folding and Self-Assembly of a Designed Peptide. J. Am. Chem. Soc. 2002; 124:15030–15037. [PubMed: 12475347]
14. Zhang S, Marini DM, Hwang W, Santoso S. Design of nanostructured biological materials through self-assembly of peptides and proteins. Curr. Opin. Chem. Biol. 2002; 6:865–871. [PubMed: 12470743]
15. Minor DL, Kim PS. Measurement of the β-sheet-forming propensities of amino acids. Nature. 1994; 367:660–663. [PubMed: 8107853]
16. Smith CK, Withka JM, Regan L. A thermodynamic scale for the β-sheet forming tendencies of the amino acids. Biochemistry. 1994; 33:5510–5517. [PubMed: 8180173]
17. Krattiger P, Kovasy R, Revell JD, Ivan S, Wennemers H. Increased Structural Complexity Leads to Higher Activity: Peptides as Efficient and Versatile Catalysts for Asymmetric Aldol Reactions. Org. Lett. 2005; 7:1101–1103. [PubMed: 15760149]
18. Tang Z, et al. Small Peptides Catalyze Highly Enantioselective Direct Aldol Reactions of Aldehydes with Hydroxyacetone: Unprecedented Regiocontrol in Aqueous Media. Org. Lett. 2004; 6:2285–2287. [PubMed: 15200341]
19. Kodaka M. Hydrolysis of p-Nitrophenyl Esters by Histidine-containing Linear and Cyclic peptides. Bull. Chem. Soc. Jpn. 1983; 56:3857–3858.
20. Bolon DN, Mayo S. Enzyme-like proteins by computational design. Proc. Natl. Acad. Sci. U.S.A. 2001; 98:14272–14279.
21. Wei Y, Hecht MH. Enzyme-like proteins from an unselected library of designed amino acid sequences. Protein Eng. Des. Sel. 2004; 17:67–75. [PubMed: 14985539]
22. Patel SC, Bradley LH, Jinadasa SP, Hecht MH. Cofactor binding and enzymatic activity in an unevolved superfamily of de novo designed 4-helix bundle proteins. Protein Sci. 2009; 18:1388–1400. [PubMed: 19544578]
23. Broo KS, Brive L, Ahlberg P, Baltzer L. Catalysis of hydrolysis and transesterification reactions of p-nitrophenyl esters by a designed helix-loop-helix dimer. J. Am. Chem. Soc. 1997; 119:11362–11372.
24. Zastrow ML, Peacock AFA, Stuckey JA, Pecoraro VL. Hydrolytic catalysis and structural stabilization in a designed metalloprotein. Nat. Chem. 2012; 4:118–123. [PubMed: 22270627]
25. Der BS, Edwards DR, Kuhlman B. Catalysis by a de novo zinc-mediated protein interface: implications for natural enzyme evolution and rational enzyme engineering. Biochemistry. 2012; 51:3933–3940. [PubMed: 22510088]

26. Verpoort JA, Mehta S, Edsall JT. Esterase activities of human carbonic anhydrases B and C. J. Biol. Chem. 1967; 242:4221–4229. [PubMed: 4964830]
27. Calero, M.; Gasset, M. Fourier Transform Infrared and Circular Dichroism Spectroscopies for Amyloid Studies. In: Sigurdsson, EM., editor. Methods Mol. Biol. Vol. Vol. 299. 2005. p. 129-151.
28. Yamaguchi K, Kamatari YO, Fukuoka M, Miyaji R, Kuwata K. Nearly Reversible Conformational Change of Amyloid Fibrils as Revealed by pH-Jump Experiments. Biochemistry. 2013; 52:6797–6806. [PubMed: 24000807]
29. Yamaguchi K, Matsumoto T, Kuwata K. Critical region for amyloid fibril formation of mouse prion protein: unusual amyloidogenic properties of the helix 2 peptide. Biochemistry. 2008; 47:13242–13251. [PubMed: 19053276]
30. Coleman JE, Coleman RV. Magnetic Circular Dichroism of Co(II) Carbonic Anhydrase. J. Biol. Chem. 1972; 247:4718–4728. [PubMed: 4626366]
31. Spevacek AR, et al. Zinc drives a tertiary fold in the prion protein with familial disease mutation sites at the interface. Structure. 2013; 21:236–246. [PubMed: 23290724]
32. Walter ED, Stevens DJ, Visconte MP, Millhauser GL. The prion protein is a combined zinc and copper binding protein: Zn^{2+} alters the distribution of Cu^{2+} coordination modes. J. Am. Chem. Soc. 2007; 129:15440–15441. [PubMed: 18034490]
33. Donnelly PS, Xiao Z, Wedd AG. Copper and Alzheimer's disease. Curr. Opin. Chem. Biol. 2007; 11:128–133. [PubMed: 17300982]
34. Chassaing S, et al. Copper and heme-mediated Abeta toxicity: redox chemistry, Aβ oxidations and anti-ROS compounds. Curr. Top. Med. Chem. 2012; 12:2573–2595. [PubMed: 23339309]
35. Cassagnes, L.-Et, et al. The Catalytically Active Copper-Amyloid-Beta State: Coordination Site Responsible for Reactive Oxygen Species Production. Angew. Chem. Int. Ed. 2013; 52:11110–11113.
36. Korendovych IV, et al. Computational Design of a Self-Assembling β-Peptide Oligomer. Org. Lett. 2010; 12:5142–5145. [PubMed: 20945888]
37. Kuipers BJH, Gruppen H. Prediction of Molar Extinction Coefficients of Proteins and Peptides Using UV Absorption of the Constituent Amino Acids at 214 nm To Enable Quantitative Reverse Phase High-Performance Liquid Chromatography–Mass Spectrometry Analysis. J. Agricult. Food Chem. 2007; 55:5445–5451.

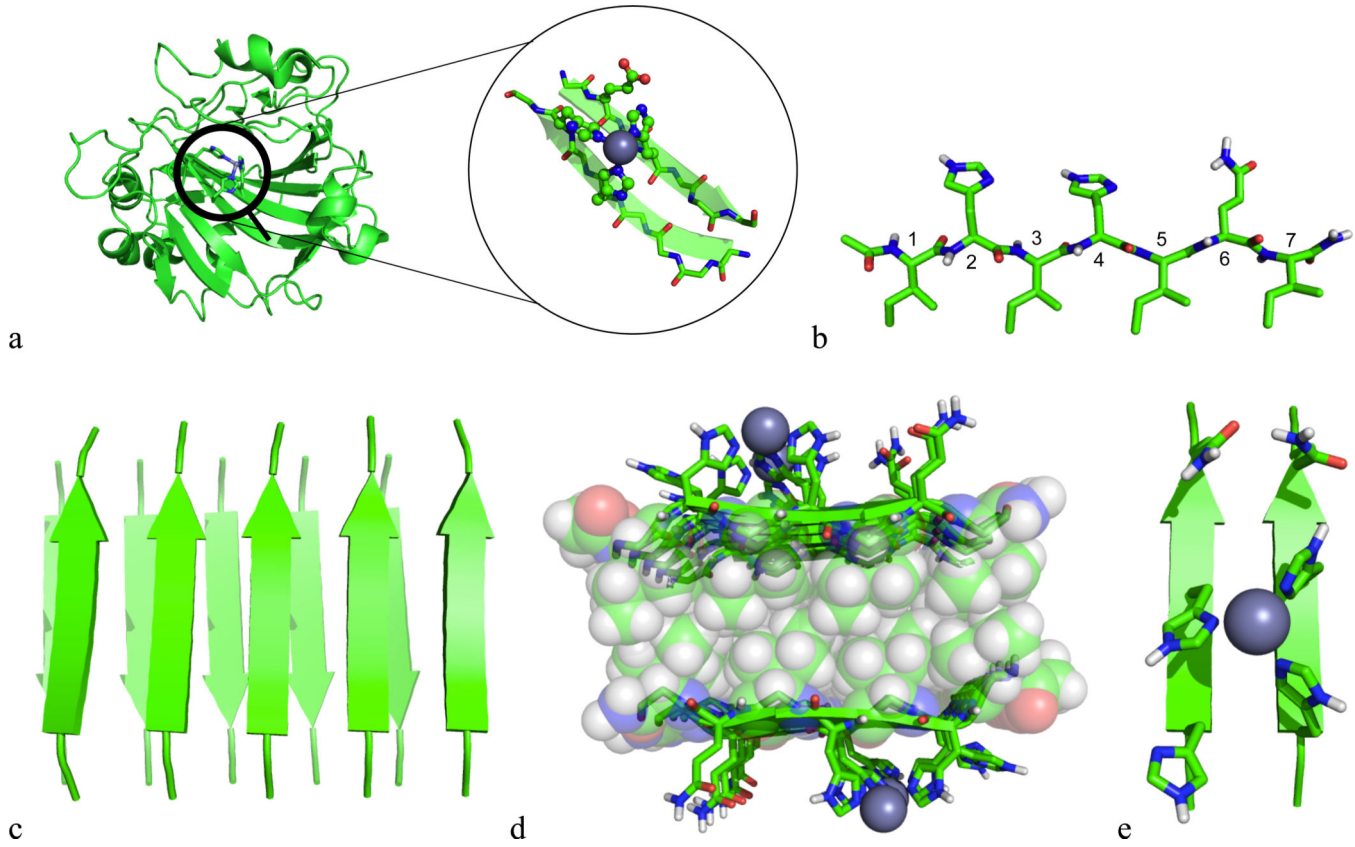

Figure 1. Overview of the concept and design

a) The structure of human carbonic anhydrase showing a typical metal-binding motif. b) A model for one of the designed peptides (**11,** Ac-IHIHIQI-$CONH_2$) in the extended β-strand configuration showing positions of the residues in the sequence. Computationally derived model of fibrils formed by **11**, showing overall fold (c), packing of the hydrophobic core (d), and zinc primary coordination sphere (e).

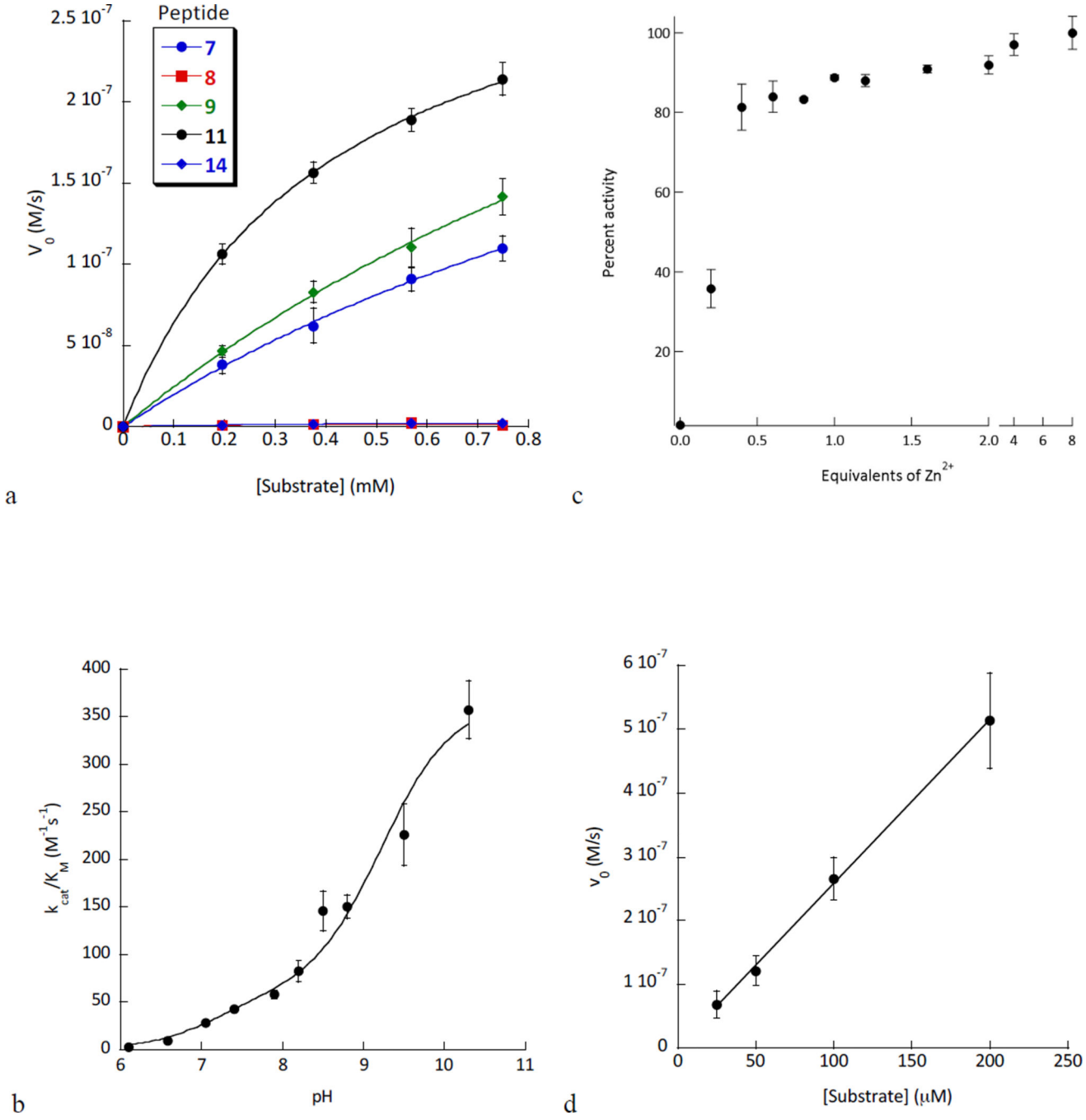

Figure 2. Functional characterization of the catalysts

a) Plots for esterase activity catalyzed by representative peptides (**7, 8, 9, 11**, and **14** as specified in the inset) at pH 8 in the presence of 1 mM Zn^{2+}, with the smooth curve showing the fit to the Michaelis-Menten equation. Profile of the most active peptide (**11**) shows an enzyme-like saturation at higher substrate concentrations. b) pH profile of esterase activity of **11** is consistent with a two-state protonation model. c) Dependence of activity of **11** on the concentration of Zn^{2+} shows a 2:1 peptide:metal stoichiometry. d) Dependence of p-nitrophenyl acetate (pNPA) hydrolysis rate catalyzed by **11** (Ac-IHIHIQI-$CONH_2$) on the

concentration of monomeric peptide used to make fibrils. Catalytic efficiency of the fibrils does not depend on the initial concentration of the monomeric peptide used for assembly; the reaction is first order in peptide in the concentration range studied. Error bars in all graphs represent standard deviations of at least three independent measurements.

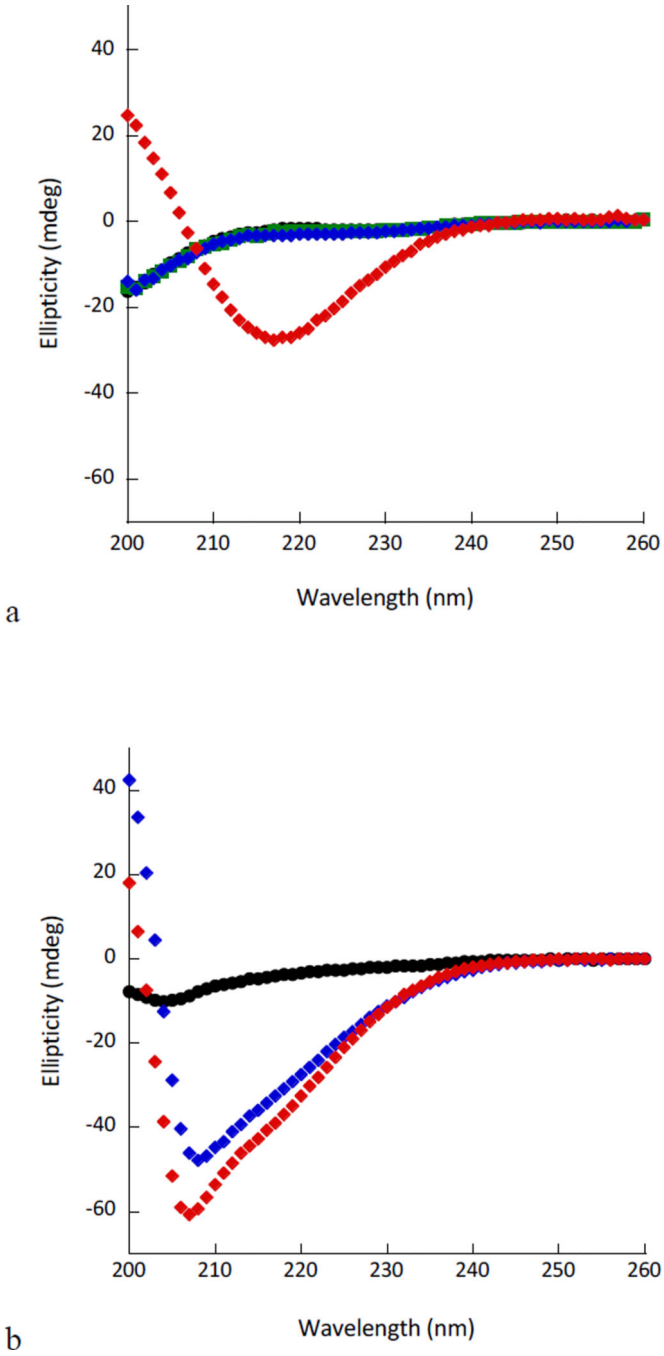

Figure 3. The active species have β-sheet secondary structure

CD spectra of **7** (a) and **11** (b) under different conditions: pH 2 – black circles; pH 2 in the presence of 1 mM $ZnCl_2$ – green squares; pH 8 – blue rhombs; pH 8 in the presence of 1 mM $ZnCl_2$ – red rhombs. In the presence of Zn^{2+} **7** displayed a spectrum typical of the cross-β configuration, the most active peptide **11** showed a β-sheet-like CD spectrum at pH 8, even in the absence of the metal. Peptide concentration was 24 μM in all experiments.

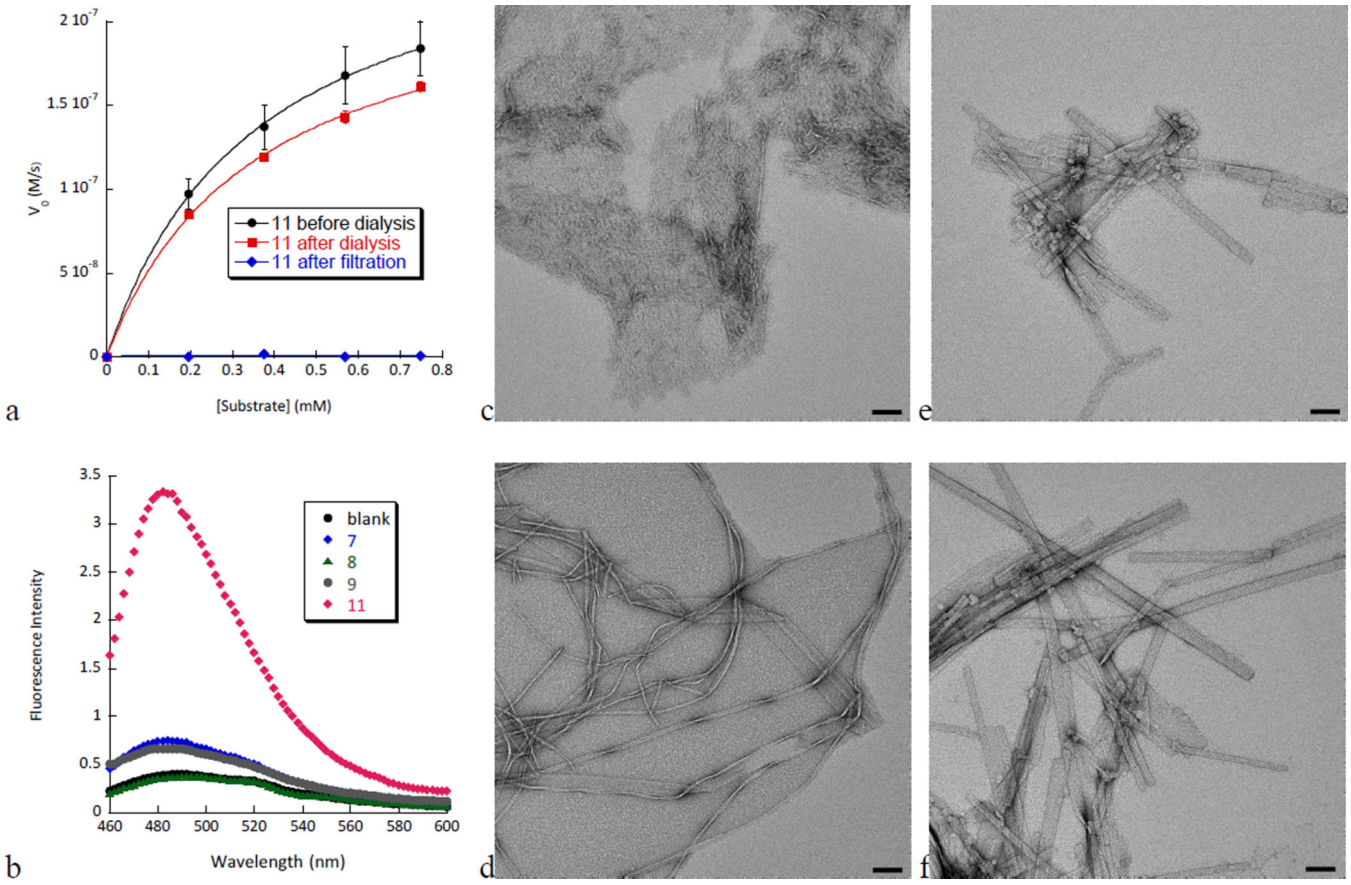

Figure 4. Large amyloid fibrils are responsible for catalysis

a) Extensive dialysis of **11** (24 μM) does not affect the activity (the observed difference in the activity is a result of partial irreversible precipitation of the fibrils as indicated by decreased UV absorbance), furthermore examination of the filtrate after passing an aqueous suspension of **11** through a 450 nm filter shows that the active species were unable to permeate the filter. b) Activity correlates with the degree of fibrillation of various peptides (**7, 8, 9** and **11** as described in the inset, peptide concentration was kept at 200 μM) as shown by thioflavin T (25 μM) fluorescence increase. Representative TEM images (at 25,000x magnification, scale bar: 100 nm) of the fibrils formed by different peptides at pH 8 in the presence of Zn^{2+}: c) **7** immediately after preparation; d) **7** after 72 hours of incubation at room temperature; e) **11** immediately after preparation; f) **11** after 72 hours of incubation at room temperature. Both **7** and **11** form amyloid-like fibrils. Freshly produced samples of **7** show protofibrils that fully mature after prolonged incubation, whereas **11** forms fibrils very quickly, essentially upon mixing. Peptide concentration was 24 μM in all TEM experiments. Error bars in all graphs represent standard deviations of at least three independent measurements.

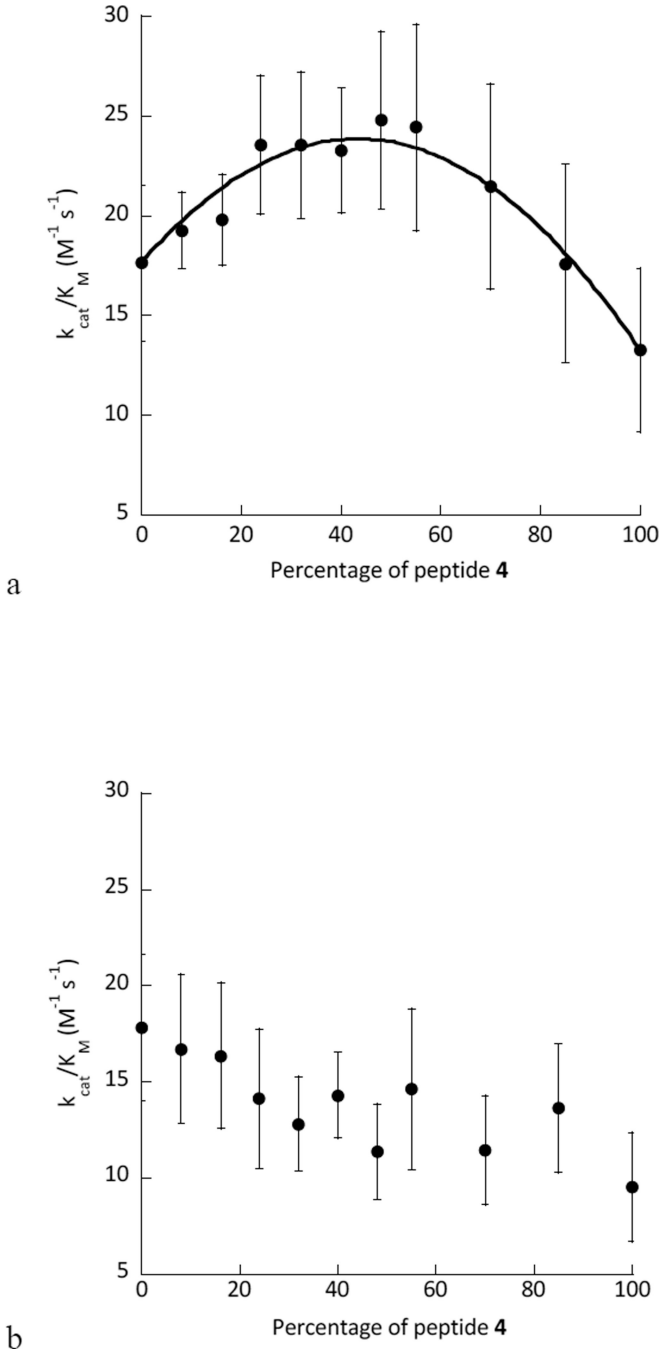

Figure 5. Synergistic interactions between peptides

a) The catalytic efficiency (k_{cat}/K_M) profile shows synergy between **4** and **7** with maximum esterase activity observed when the peptides were mixed relative to the individuals alone. The experimental data are well described by a simple model, where a dimer is the active species and the peptides are randomly distributed in the fibril (fit). b) No synergy is observed when preformed fibrils of **4** and **7** are mixed together, instead a linear decrease in activity was seen upon increasing the ratio of **4** relative to **7** Conditions: pH 8, total peptide concentration was kept at 24 μM, the buffer contained 1 mM Zn^{2+}, the fibrils were

equilibrated for 48 hours prior to measurements. Error bars in all graphs represent standard deviations of at least three independent measurements.

Table 1

Esterase activity for the designed peptides at pH 8 in the presence of 1 mM Zn^{2+}.

Peptide	Sequence	k_{cat}/K_M, M^{-1} s^{-1}	$k_{cat}\times10^{-2}$, s^{-1}	K_M, mM
Position 6 variants				
1	Ac-LHLHLDL-$CONH_2$	0.2 ± 0.1		
2	Ac-LHLHLEL-$CONH_2$	< 0.2		
3	Ac-LHLHLQL-$CONH_2$	30 ± 3		
4	Ac-LHLHLYL-$CONH_2$	13 ± 5		
5	Ac-LHLHLHL-$CONH_2$	0.60 ± 0.08		
6	Ac-LHLHLKL-$CONH_2$	12 ± 2		
7	Ac-LHLHLRL-$CONH_2$	18 ± 4		
Leucine substitutions				
7	Ac-LHLHLRL-$CONH_2$	18 ± 4	3.2 ± 0.4	1.8 ± 0.4
8	Ac-AHAHARA-$CONH_2$	0.12 ± 0.8		
9	Ac-IHIHIRI-$CONH_2$	22 ± 8	4.2 ± 0.8	1.9 ± 0.5
10	Ac-VHVHVRV-$CONH_2$	26 ± 4	3.8 ± 0.3	1.5 ± 0.2
Combined substitutions				
11	Ac-IHIHIQI-$CONH_2$	62 ± 2	2.60 ± 0.04	0.4 ± 0.1
11a	Ac-VHVHVQV-$CONH_2$	32 ± 2	1.6 ± 0.2	0.5 ± 0.1
Primary Ligand variants				
12	Ac-IAIHIRI-$CONH_2$	0.36 ± 0.16		
13	Ac-IHIAIRI-$CONH_2$	0.2 ± 0.4		
Removal of N, C-terminal blocking groups				
14	H_2N-IHIHIQI-COOH	1 ± 3		